UNIWERSYTET JAGIELLOŃSKI KRAKÓW

Mercury dimer interatomic potentials for quantum-mechanics tests and photoassociation experiments in a MOT §

Jarosław Koperski
Instytut Fizyki, Uniwersytet Jagielloński, ul. Reymonta 4, 30-059 Kraków, Poland
E-mail: ufkopers@cyf-kr.edu.pl

Overview

Recently, a precise knowledge about potential energy (PE) curves of mercury dimer (Fig. 1) has been engaged in experiments of femtosecond photoassociation spectroscopy (Fig. 2). Photoassociation of Hg_2, femtosecond dynamics, and quantum dynamical wave packet description of these reactions [1] as well as coherent bond formation of Hg_2 obtained in the femtosecond time scale [2] have been reported. Furthermore, results of Hg_2 spectroscopy are employed in planned fundamental experimental tests of quantum mechanics, particularly a realization of EPR *gedanken*experiment and loophole-free tests of the Bell inequalities in a regime different from those using photons [3] (Fig. 3). The specific form of Hg_2 PE curves is exploited in planned experiment of the formation of Hg_2 by photoassociation in a MOT [4] (Fig. 4).

It is highly desirable to have knowledge on the accuracy of Hg_2 PE curves, especially those involved in the above considerations. Improved characteristics based on rigorous analysis of the $F0^+_u \leftarrow X0^+_g$, $D1_u \leftarrow X0^+_g$, $E1_u \rightleftarrows X0^+_g$ and $G0^+_u \rightleftarrows X0^+_g$ transitions in excitation and fluorescence spectra obtained in experiments of crossed supersonic and laser beams (Fig. 5) are presented. The results [9] considerably extend previously reported investigations [5]. A more accurate value for the R_e'' obtained from an investigation of the $G0^+_u \rightleftarrows X0^+_g$ transition [5] has been adopted in theoretical simulation of the $F0^+_u \leftarrow X0^+_g$ (Fig. 6), $E1_u \rightleftarrows X0^+_g$ (Fig. 7) and $D1_u \leftarrow X0^+_g$ (Figs. 8 and 9) transitions. New values for R_e' of the $D1_u$ and $E1_u$ states have been determined. An isotopic-shift analysis of the v'←v''=0 vibrational bands in the $D1_u \leftarrow X0^+_g$ transition (Fig. 10) provided improved $D1_u$ state characteristics. They were used in the simulation of the Fanck-Condon factors profile of the transition. A simultaneous simulation of the v'←v''=0 and v'←v''=1 vibrational progressions in the $E1_u \rightleftarrows X0^+_g$ transition provided an improved value for the $\Delta R_e = R_e' - R_e''$ (see Table).

References

[1] P. Backhaus and B. Schmidt, *Chem. Phys.* **217**, 131 (1997); P. Backhaus *et al.*, *Chem. Phys. Lett.* **306**, 18 (1999); U. Marvet *et al.*, *J. Phys. Chem. A* **102**, 4111 (1998).
[2] U. Marvet and M. Dantus, *Chem. Phys. Lett.* **245**, 393 (1995).
[3] E.S. Fry *et al.*, *Phys. Scr.* T**76**, 47 (1998); E.S. Fry and T. Walther, *Adv. At. Mol. Opt. Phys.* **42**, 1 (2000); E.S. Fry *et al.*, *Phys. Rev. A* **52**, 4381 (1995).
[4] T. Walther, Workshop on Prospects of Cold Molecules, Heidelberg, November 1999 (poster).
[5] (a) J. Koperski *et al.*, *Chem. Phys. Lett.* **219**, 161 (1994); (b) *Can. J. Phys.* **72**, 1070 (1994); (c) *J. Mol. Spectrosc.* **184**, 300 (1997).
[6] R.D. van Zee et al., *J. Chem. Phys.* **88**, 4650 (1988); A. Zehnacker *et al.*, *J. Chem. Phys.* **86**, 6565 (1987).
[7] M. Dolg and H.-J. Flad, *J. Phys. Chem.* **100**, 6147 (1996); *ibid*. **100**, 6152 (1996); *private communication*.
[8] L.J. Munro *et al.*, *J. Chem. Phys.* **114**, 5545 (2001).
[9] J. Koperski, *Habilitation Thesis*, Jagiellonian University Press, 2001.

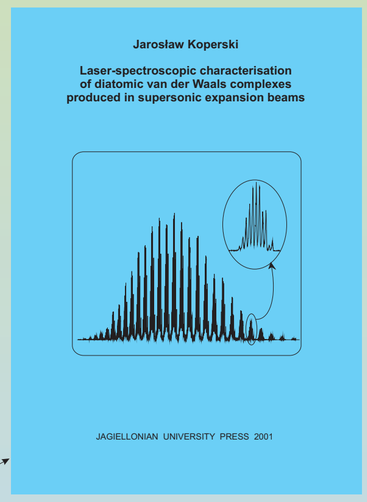

Hg_2 - Potential Energy Curves

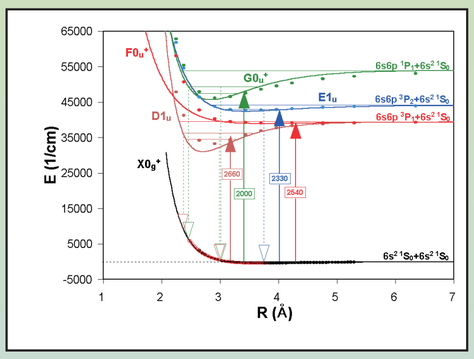

Fig. 1. A partial diagram for Hg_2 molecule showing PE curves for the ground and excited states correlated with the $6^3P_1+6^1S_0$, $6^3P_2+6^1S_0$ and $6^1P_1+6^1S_0$ atomic asymptotes. The ground-state potential is represented by a Lennard-Jones (n-6) function (n=6.21) [5(c)]. All excited-state potentials are represented by Morse functions with parameters from Ref. [9]. Solid arrows with wavelengths corresponding to the centers of absorption from the $X0^+_g$,v''=0 to the $F0^+_u(6^3P_1)$, $D1_u(6^3P_1)$, $E1_u(6^3P_2)$ and $G0^+_u(6^1P_1)$ excited states as well as fluorescence regions (broken arrows) are depicted. In the case of deeper $D1_u$ and $G0^+_u$, states a range of v'-levels probed in the excitation from the ground state (so-called FC-"window") is also shown. Full circles represent *ab initio* points of Dolg and Flad [7] (for the $X0^+_g$ state) and Czuchaj *et al.*, *Chem. Phys.* **214**, 277 (1997) (for the excited states). Open circles show a result obtained using an inverted procedure of LeRoy (see Child *et al.*, *J. Chem. Phys.* **78**, 6732 (1983)) applied to the $G0^+_u$,v'=39→$X0^+_g$ fluorescence spectrum [5(c)].

Femtosecond PhotoAssociation Spectroscopy

M. Dantus and co-workers
Michigan State University, East Lansing, MI

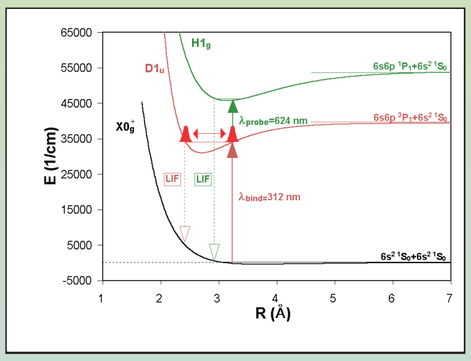

Fig. 2. FPAS experiment on Hg_2 according to Refs. [1,2]. Generally, a gas phase system has a repulsive ground state $X0^+_g$. Binding by the laser (photoassociation) is followed by excitation to a higher state $H1_g$; the evolution of the wave-packet along $D1_u$ is probed by varying the delay between λ_{bind} and λ_{probe} and monitoring the fluorescence from $H1_g$ or the depletion of the fluorescence from $D1_u$. In real system, the initial pulse photoassociates Hg_2 in the $D1_u$ state; the depletion of the $D1_u \rightarrow X0^+_g$ fluorescence is monitored as λ_{probe} causes excitation to the $H1_g$ state. The photoassociation yield of Hg atoms to produce excited Hg_2 is enhanced for short (ps) and for ultrashort (fs) pulse durations. Ultrashort laser pulses effectively overlap the entire range of free-bound transition achieving maximum probability (after Refs. [1,2]).

EPR *gedanken*experiment and Bell inequalities

E. S. Fry and Th. Walther
Texas A&M University, College Station, TX

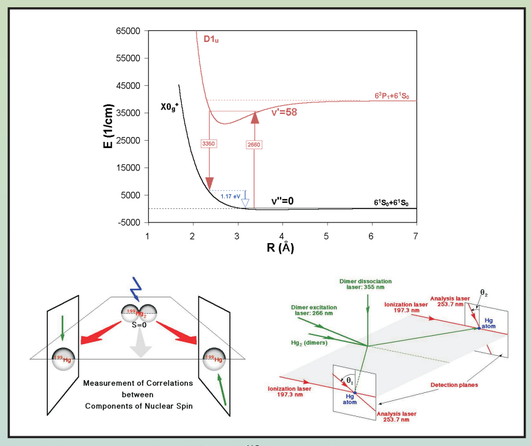

Fig. 3. Generation of an $|\Psi\rangle = 1/2^{1/2}\{|\uparrow\rangle_1|\downarrow\rangle_2 - |\downarrow\rangle_1|\uparrow\rangle_2\}$ entangled state by a dissociation of $^{199}Hg_2$ dimers in a supersonic beam with a total nuclear spin S=0 (each of the ^{199}Hg atom has nuclear spin I=1/2) using relevant $D1_u$,v'=58←$X0^+_g$,v''=0 bound-bound (2660 Å) and $D1_u$,v'=58→$X0^+_g$ bound-free (3550 Å) stimulated-Raman transitions. Produced entangled atoms are spatially separated and due to the momentum conservation they will fly apart in exactly opposite directions in the center-of-mass frame. Determination of the correlation in the spin components of the two entangled atoms as well as detection of the atoms is achieved via a state-selective two-photon excitation-ionization scheme (after Ref. [3]).

Trapping of neutral Hg_2 in a MOT

Th. Walther and E. S. Fry
Texas A&M University, College Station, TX

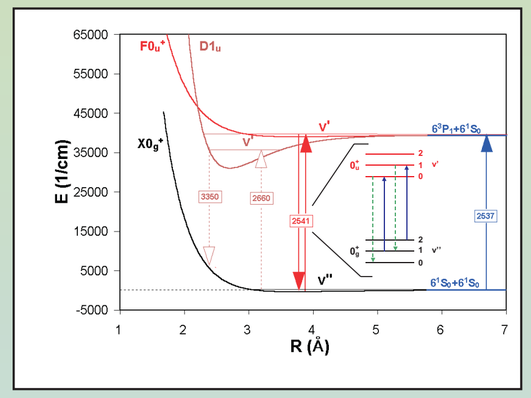

Fig. 4. Formation of ultra-cold molecules in a MOT by photo-associative spectroscopy [4]. The dimer forming process starts upon a collision of two trapped ground-state Hg atoms. Due to the photoassociation laser (λ=2537 Å) they will undergo a free-bound transition into a vibrationally excited state of the $F0^+_u$ or the $D1_u$ states, from where they will decay back down to bound or free states of the $X0^+_g$ ground state (those decaying to free states will be lost due to radiative escape). The $F0^+_u \rightleftarrows X0^+_g$ in the dimer is strongly allowed (see Ref. [5(a)]), which should favor bound-bound transitions. These will cause a vibrational cooling shown in insert (λ=2541 Å - repumping laser). Transitions λ=2660 Å and λ=3350 Å: scheme for detection of Hg_2 by laser induced fluorescence is shown with brown dashed arrows (after Ref. [4]).

Experimental Setup

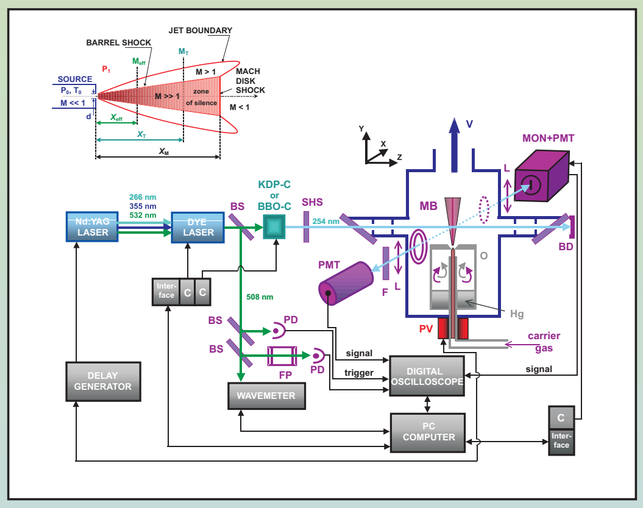

Fig. 5. Schematic layout of the apparatus [5,9]. **O**-stainless-steel oven; **PV**-pulsed valve; **MB**-molecular beam; **V**-vacuum pump system; **KDP-C** or **BBO-C**-second or third harmonic generator; **BS**-beam splitters; **SHS**-second harmonic selector; **C**-scanning controllers; **FP**-Fabry-Perot interferometer; **PD**-photodiodes; **PMT**-photomultiplier tube; **MON**-monochromator; **F**-filter; **L**-lens; **BD**-beam dump.

Hg_2 Excitation Spectrum of the $F0^+_u(6^3P_1) \leftarrow X0^+_g(6^1S_0)$ Transition

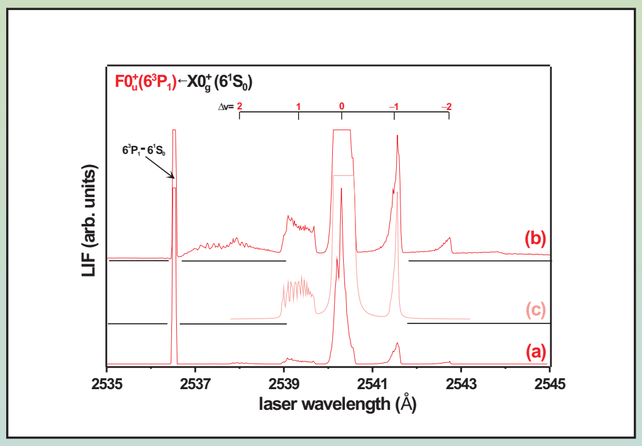

Fig. 6. $F0^+_u(6^3P_1) \leftarrow X0^+_g(6^1S_0)$ excitation spectrum of Hg_2 reported in Ref. [5(a)] showing $\Delta v = 0, \pm 1, \pm 2$ sequences recorded with **(a)** low and **(b)** high sensitivity of the detection system. **(c)** Trace showing a computer-simulated spectrum of the $\Delta v = 0, \pm 1$ sequences assuming a Lennard-Jones (n-6), n=6.21, function for the ground-state potential (R_e''=3.69 Å) and a Morse representation for the excited-state potential (R_e'=3.66 Å).

Hg_2 Excitation Spectrum of the $E1_u(6^3P_2) \leftarrow X0^+_g(6^1S_0)$ Transition

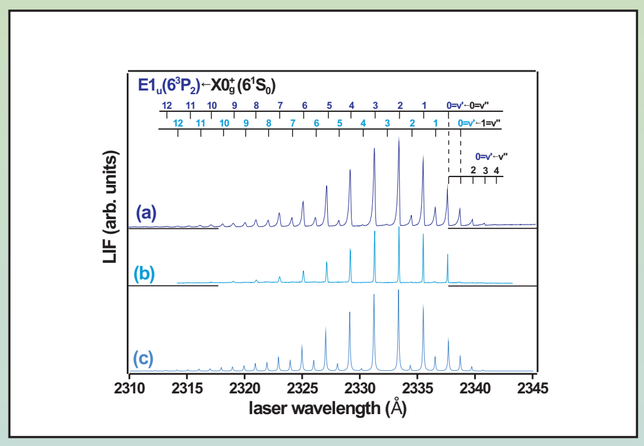

Fig. 7. (a)-(b) $E1_u(6^3P_2) \leftarrow X0^+_g(6^1S_0)$ excitation spectrum of Hg_2 reported in Ref. [5(b)] showing the v'←v''=0 and v'←v''=1 progressions. A partial v'=0←v'' "hot" progression is present in **(a)**. **(c)** Trace with a computer-simulated spectrum of both v'←v''=0 and v'←v''=1 progressions assuming a Lennard-Jones (n-6), n=6.21 function for the ground state potential (R_e''=3.69 Å) and a Morse representation for the excited state potential (R_e'=3.445 Å).

Hg_2 Excitation Spectrum of the $D1_u(6^3P_1) \leftarrow X0^+_g(6^1S_0)$ Transition

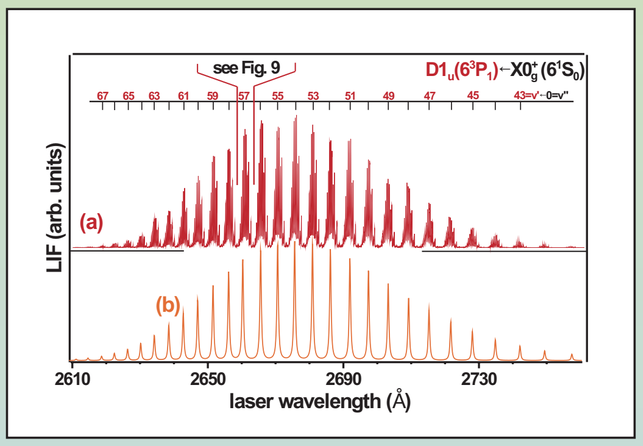

Fig. 8. (a) $D1_u(6^3P_1) \leftarrow X0^+_g(6^1S_0)$ excitation spectrum of Hg_2 reported in Ref. [5(b)] showing the v'←v''=0 progression. An isotopic structure of each of the v'-component was resolved in the experiment [5(b)] and analyzed [9]. **(b)** Lower trace shows a computer-simulated spectrum (LEVEL 6.1 code http://theochem.uwaterloo.ca/~leroy of LeRoy) of the v'←v''=0 progression for the (m_1+m_2)=401 isotopic peaks assuming a Lennard-Jones (n-6) ground-state potential with n=6.21 and R_e''=3.69 Å, and a Morse potential with R_e'=2.71 Å for the excited state. Detailed view of the v'=57←v''=0 component is shown in Fig. 9. An isotopic-shift analysis is presented in Fig. 10.

$D1_u$, v'=57←$X0^+_g$, v''=0 component

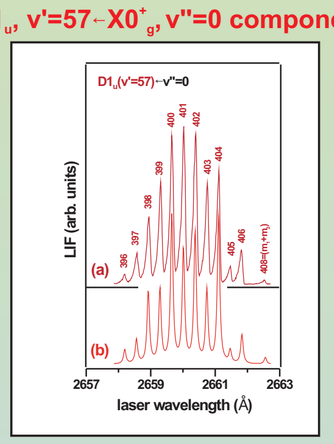

Fig. 9. (a) The isotopic structure of the $D1_u$,v'=57←$X0^+_g$,v''=0 vibrational component recorded in Ref. [5(b)]. **(b)** Trace representing a simulation of the isotopic structure. The position of the central (m_1+m_2)=401 peak was obtained using LEVEL 6.1 code and the relative positions of the isotopic peaks were calculated using Eq. (1). Their amplitudes were weighted relative to the isotopic abundances in natural mercury. The individual isotopic peaks were represented by a Lorentzian convolution function with FWHM of 2.5 cm^{-1}. It should be noted that the individual experimental peaks are "blue-shaded" due to the unresolved rotational structure and considerably large width of the Lorentzian representation does not reflect the real breadth of the isotope component.

Isotopic-shift analysis

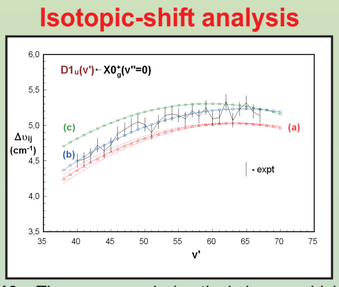

Fig. 10. The measured (vertical bars, which also correspond to the experimental error) and **(a)-(c)** calculated isotopic shifts $\Delta\upsilon_{ij}$ of the $D1_u \leftarrow X0^+_g$,v''=0 vibrational progression of Ref. [5(b)]. **(a)** The $\Delta\upsilon_{ij}(v')$ dependence plotted according to the result of author's earlier investigation [5(b)] assuming the v'±1 assignment (triangles, red dashed line). **(b)** Result of an improved characterization of the $D1_u \leftarrow X0^+_g$,v''=0 vibrational progression (diamonds, blue solid line) in which the isotope structure was taken into consideration (note that the $\Delta\upsilon_{ij}(v')$ dependency was not analyzed in Ref. [5(b)]). **(c)** $\Delta\upsilon_{ij}(v')$ plotted according to the result of Zehnacker *et al.* [6] (squares, green solid line). An expression for isotope shift, $\Delta\upsilon_{ij}$, in v'←v''=0 vibronic transitions between components corresponding to the various (m_1+m_2) combinations of the isotope masses present in natural elements of the molecule:

$$\Delta\upsilon_{ij}(v') = (1-\rho)\,\omega_e'(v'+1/2) - (1-\rho^2)\,\omega_e'x_e'(v'+1/2)^2 - (1-\rho)\,\omega_e''/2 + (1-\rho^2)\,\omega_e''x_e''/4, \qquad (1)$$

where $\rho = (\mu/\mu_i)^{1/2}$ and $\mu = m_1m_2/(m_1+m_2)$.

Results

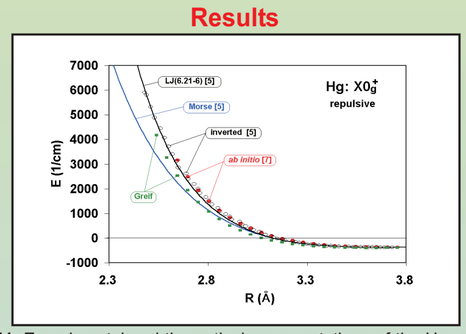

Fig. 11. Experimental and theoretical representations of the Hg_2 ground-state potential for the short-range region. The potentials, as well as points from RKR-like inversion method obtained in Ref. [5(c)] are compared with the result of *ab initio* calculation [7] and points of Greif from Raman spectroscopy of Hg_2 (J.N. Greif-Wüstenbecker, *Ph.D. Thesis*, Philipps-Universität Marburg, 2000).

	$X0^+_g$	$F0^+_u$	$D1_u$	$E1_u$
D_e	380±15 [5]; 379.1 [7]	432±10 [5]; 410±20 [6]	**8385±10** [9]; 8100±200 [5]	1660±40 [5]
ΔR_e	3.69±0.01 [5] 3.63±0.01 [6]; 3.730 [7]	3.66±0.04 [5] 3.61±0.5 [6]	**2.710±0.005** [9]	**3.445±0.002** [9] 3.38±0.04 [5]
R_e	–	0.030±0.002 [5]	**–0.980±0.005** [9]	**–0.245±0.002** [9] –0.250±0.004 [5]
B_e	**0.0123±0.0001** [9] 0.0127±0.0003 [6] 0.0122±0.0003 [8]	–	**0.0228±0.0001** [9]	–
ω_e	19.6±0.3 [5] 19.7±0.5 [6]; 19.6446 [8]	18.6±0.4 [5] 18.5±0.5 [6]	**129.5±0.3** [9] 127.0±0.6 [5]	40.2±0.3 [5]
$\omega_e x_e$	0.26±0.03 [5] 0.27 [6]; 0.2265 [8]	0.20±0.02 [5] 0.21 [6]	0.50±0.01 [5]	0.18±0.02 [5]

Acknowledgments

§ Supported by the State Committee for Scientific Research, KBN, Grant 5 P03B 037 20